STRUCTURAL CONTROL AND HEALTH MONITORING
Struct. Control Health Monit. 2008; **15**:657–672
Published online 8 July 2008 in Wiley InterScience
(www.interscience.wiley.com). DOI: 10.1002/stc.267

Smart base-isolated benchmark building part IV: Phase II sample controllers for nonlinear isolation systems

S. Narasimhan[1,‡], S. Nagarajaiah[2,*,†,§] and E. A. Johnson[3,¶]

[1]*Department of Civil and Environmental Engineering, University of Waterloo, Waterloo, Ont., Canada*
[2]*Department of Civil and Environmental Engineering and Mechanical Engineering and Materials Science, Rice University, Houston, TX 77005, U.S.A.*
[3]*Department of Civil and Environmental Engineering, University of Southern California, Los Angeles, CA, U.S.A.*

SUMMARY

The first phase of the seismically excited base-isolated benchmark building was received well by the structural control community, culminating in the March 2006 journal special issue. The special issue contained contributions from over dozen participants world-wide. While the focus of the Phase I effort was on linear isolation systems, Phase II attempts to galvanize research efforts on control of base-isolated buildings with nonlinear isolation systems. Primarily, friction and hysteretic lead–rubber-bearing (LRB) isolation systems are included in this effort. The superstructure and the control framework remains the same as the Phase I benchmark. The main difference will be in the nonlinear isolation systems used, and consequently the controllers necessary to control such systems. The primary objective of this paper is to present the Phase II benchmark problem definition along with a sample controller for friction isolation system. A sample controller for the LRB isolation system was presented earlier as a part of the Phase I special issue. Included in this paper is a broad set of carefully chosen performance measures, which remain the same as Phase I, so that the participants may evaluate their respective control designs. The control algorithms may be passive, active or semiactive. The benchmark structure considered in the Phase II study is an eight-story base-isolated building that is identical to the one considered for the Phase I study. The base isolation system consists of a combination of linear, nonlinear bearings and control devices. The superstructure is considered to be a linear elastic system with lateral–torsional behavior. The nonlinearities due to the isolators and control devices are limited to the isolation level only. A nonlinear dynamic analysis program and sample controllers are made available to the participants to facilitate direct comparison of results of different control algorithms. Copyright © 2008 John Wiley & Sons, Ltd.

KEY WORDS: smart base-isolated building benchmark; structural control; nonlinear isolation systems

*Correspondence to: S. Nagarajaiah, Department of Civil and Environmental Engineering and Mechanical Engineering and Materials Science, 6100 S. Main Street, Rice University, Houston, TX 77005, U.S.A.
†E-mail: nagaraja@rice.edu
‡Assistant Professor.
§Professor.
¶Associate Professor.

Contract/grant sponsor: National Science Foundation
Contract/grant sponsor: University of Waterloo
Contract/grant sponsor: Natural Sciences and Engineering Research Council (NSERC) of Canada

Received 16 May 2007
Revised 22 February 2008
Accepted 3 March 2008

1. INTRODUCTION

Recently, well-defined analytical benchmark problems [1–7] have been developed for studying response control strategies for building and bridge structures subjected to seismic and wind excitation, by broad consensus effort of the American Society of Civil Enigneers (ASCE) structural control committee. The goal of this effort was to develop benchmark models to provide systematic and standardized means by which competing control strategies, including devices, algorithms, sensors, etc., can be evaluated. Carefully defined analytical benchmark problems are an excellent alternative to expensive experimental benchmark test structures. Owing to the effectiveness of the fixed-base building benchmark effort [4,5,7], the ASCE structural control committee voted to develop a new smart base-isolated benchmark problem. Owing to the complexity and the wide range of isolation systems proposed for the smart base-isolated benchmark, two phases for the study were proposed. The focus of Phase I was on linear isolation systems [3,8,9], which was received well by the structural control community culminating in the recent special issue that appeared in the Journal of Structural Control and Health Monitoring [3,8,9]. In Phase II of the benchmark study, an identical benchmark superstructure is considered with nonlinear isolation systems. The nonlinear isolation system consists of a combination of linear and hysteretic (friction and lead–rubber) bearings along with nonlinear control devices. The superstructure is linear with lateral–torsional behavior and the nonlinearities arising from the nonlinear bearing and device characteristics are limited to the isolation level only.

Base isolation systems such as sliding and elastomeric-bearing systems reduce the superstructure response, but with increased base displacements in near-fault earthquake ground motions [10,11]. Current practice is to provide nonlinear passive dampers to limit the bearing displacements; however, this increases the forces in the superstructure and at the isolation level. In order to mitigate this problem, control devices such as active and semiactive devices are placed at the isolation level [10–21]. For linear isolation systems, concepts of controller synthesis are well understood [12,22,23]. Various control methods utilizing concepts of linear optimal control theory have been proposed and verified by researchers. This is in part reflected by an overwhelming participation for the Phase I benchmark study dedicated to the study of linear isolation systems. On the other hand, control of nonlinear base-isolated systems presents significant challenges. For example, widely utilized concepts of optimal control are not applicable to control nonlinear systems. Researchers have proposed several techniques utilizing linearization, nonlinear control, adaptive control and neural networks to achieve this objective. In spite of this, there are several issues to be addressed with regard to nonlinear systems, and presents a challenging problem. For example, state estimation, techniques for which are well understood for linear systems, poses several difficulties for nonlinear systems. Coupled with system uncertainty, we have a system that poses considerable theoretical difficulties and practical implementation issues. The goal of achieving a single or a set of effective nonlinear controllers that address many of the practical challenges, similar to those of linear systems, still remains elusive for such systems. Nevertheless, results from several recent studies, e.g. [16,18], are indicative of the research potential that exists in developing new strategies. In light of this, the main focus of the Phase II benchmark effort is to galvanize the efforts of the structural control community toward addressing this challenging problem of nonlinear control of base-isolated buildings. It is anticipated that the contributions from various participants would further the current understanding in the control of nonlinear base-isolated systems.

DOI: 10.1002/stc

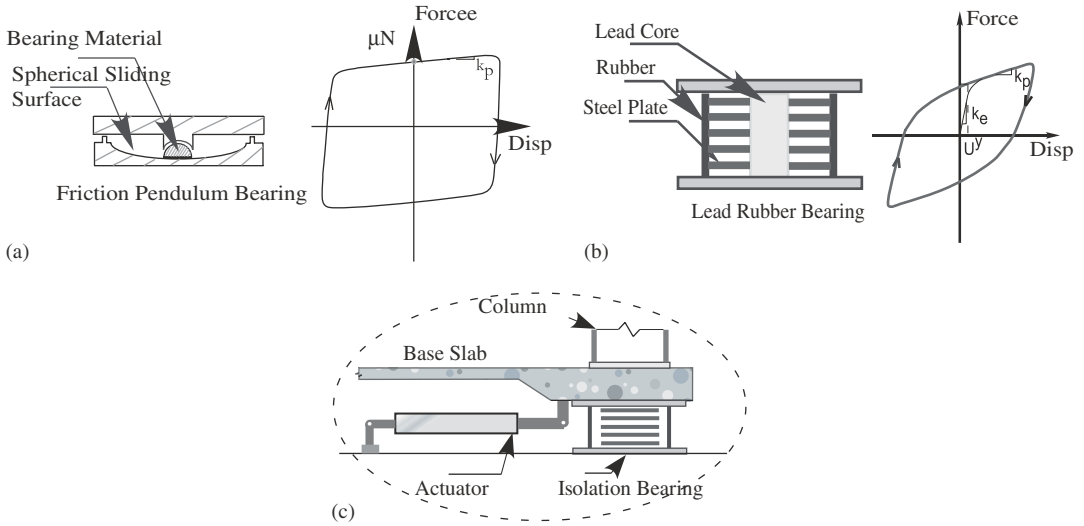

Figure 1. Isolation types in Phase II: (a) friction pendulum system; (b) lead–rubber bearing; and (c) isolation and device placement.

There are two isolation systems considered in this study as shown in Figure 1: the friction pendulum system and the lead–rubber-bearing (LRB) system. Both the isolation systems exhibit nonlinear hysteretic behavior. The control devices can be placed only at the isolation level. The objective of this study is to invite participants to propose novel and effective control designs that result in reduced base displacements, superstructure responses and isolation level forces for the structure. A set of evaluation criteria have been presented for the sake of comparison of various control strategies. In addition, sample controllers have been provided for the semiactive control of nonlinear friction isolation system using magnetorheological (MR) dampers [24]. The sample controller for hysteretic LRB isolation system has already been included in the Phase I special issue [9]. The control devices for the sample controller presented in this study are installed at the isolation level between the base and the foundation at eight locations (Figure 2), each location consisting of a single orthogonal pair to control the responses in both directions. The controllers developed herein are not intended to be competitive; they are intended to serve as a guide for participants to design competitive controllers for the nonlinear base-isolated building benchmark.

2. STRUCTURAL AND ISOLATION MODEL

The benchmark structure is a base-isolated eight-story, steel-braced framed building, 82.4-m long and 54.3-m wide, identical to the one considered for the Phase I study [3]. The floor plan is L-shaped as shown in Figure 2. The superstructure bracing is located at the building perimeter. Metal decking and a grid of steel beams support all concrete floor slabs. The steel superstructure is supported on a reinforced concrete base slab, which is integral with concrete beams below, and drop panels below each column location. The isolators are connected between these drop

DOI: 10.1002/stc

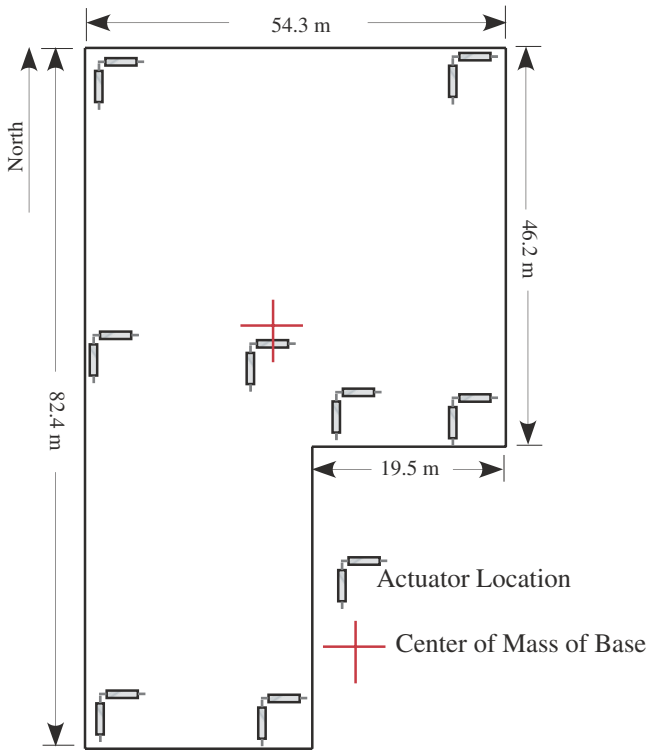

Figure 2. Actuator locations distributed in the base of the structure.

panels and the footings below as shown in Figure 1(c). The superstructure is modeled as a three-dimensional linear elastic system. The superstructure members, such as beam, column, bracing and floor slab, are modeled in detail (Figure 2). Floor slabs and the base are assumed to be rigid in plane. The superstructure and the base are modeled using three master degrees of freedom (DOF) per floor at the center of mass. The combined model of the superstructure (24 DOF) and the isolation system (3 DOF) consists of 27 DOF. All twenty-four modes in the fixed-base case are used in modeling the superstructure. The superstructure damping ratio is assumed to be 5% in all fixed-base modes. The computed natural periods for the first nine fixed-base modes are 0.78, 0.27 and 0.15 s in the North–South direction, 0.89, 0.28 and 0.15 s in the East–West direction and 0.66, 0.21 and 0.12 s in torsion. The nominal isolation system consists of 61 nonlinear isolation bearings (friction pendulum or LRB) and 31 linear elastomeric bearings.

The biaxial hysteretic behavior of LRBs and frictional bearings is modeled using the biaxial interaction equations of Bouc–Wen model [25,26] as follows:

$$U^{y}\begin{Bmatrix} \dot{z}_x \\ \dot{z}_y \end{Bmatrix} = \alpha\begin{Bmatrix} \dot{U}_x \\ \dot{U}_y \end{Bmatrix} - \mathbf{Z}_w\begin{Bmatrix} \dot{U}_x \\ \dot{U}_y \end{Bmatrix}$$

$$\mathbf{Z}_w = \begin{bmatrix} z_x^2(\gamma\ \mathrm{sgn}(\dot{U}_x z_x) + \beta) & z_x z_y(\gamma\ \mathrm{sgn}(\dot{U}_y z_y) + \beta) \\ z_x z_y(\gamma\ \mathrm{sgn}(\dot{U}_x z_x) + \beta) & z_y^2(\gamma\ \mathrm{sgn}(\dot{U}_y z_y) + \beta) \end{bmatrix} \tag{1}$$

DOI: 10.1002/stc

where z_x and z_y are dimensionless hysteretic variables that are bounded by values ± 1, α, β and γ are dimensionless quantities, U_x, U_y and $\dot{U}_x$, $\dot{U}_y$ represent the displacements and velocities in the x and y directions, respectively, at the isolation bearing or device. When yielding commences Equation (1) leads to $z_x = \cos\theta$ and $z_y = \sin\theta$ provided $\alpha/(\beta+\gamma) = 1$ with $\theta = \tan^{-1}(\dot{U}_x/\dot{U}_y)$ and resultant velocity $\dot{U} = \sqrt{\dot{U}_x^2 + \dot{U}_y^2}$. The biaxial interaction can be neglected when the off-diagonal terms of the matrix in Equation (1) are replaced by zeros. This results in an uniaxial model with two independent elements in two orthogonal directions. The forces, f, mobilized in the elastomeric isolation bearings or devices can be modeled by a elasticviscoplastic model with strain hardening:

$$f_x = k_{\mathrm{p}} U_x + c_{\mathrm{v}} \dot{U}_x + (k_{\mathrm{e}} - k_{\mathrm{p}}) U^{\mathrm{y}} z_x \tag{2}$$

$$f_y = k_{\mathrm{p}} U_y + c_{\mathrm{v}} \dot{U}_y + (k_{\mathrm{e}} - k_{\mathrm{p}}) U^{\mathrm{y}} z_y \tag{3}$$

where k_{e} is the pre-yield stiffness, k_{p} the post-yield stiffness, c_{v} the viscous damping coefficient of the elastomeric bearing or device and U^{y} the yield displacement.

Equation (1) can also be used to model sliding bearings with flat or spherical sliding surface, by means of a small yield displacement U^{y} (because of rigid plastic behavior and large pre-yield stiffness) setting $c_{\mathrm{v}} = 0$ and $(k_{\mathrm{e}} - k_{\mathrm{p}})U^{\mathrm{y}} = \mu N$:

$$f_x = k_{\mathrm{p}} U_x + \mu N z_x \tag{4}$$

$$f_y = k_{\mathrm{p}} U_y + \mu N z_y \tag{5}$$

where μ is the coefficient of friction and N is the average normal force at the bearing (normal force variation is neglected). In a similar manner other devices such as nonlinear fluid dampers can also be modeled using Equation (1).

3. THREE-DIMENSIONAL NONLINEAR DYNAMIC ANALYSIS

Base-isolated buildings are designed such that the superstructure remains elastic. Hence, in this study the superstructure is modeled by a condensed linear elastic system. In addition, the equations of motion are developed in such a way that the fixed-base properties are used for modeling the linear superstructure. The base and the floors are assumed to be infinitely rigid in plane. The superstructure and the base are modeled using three master DOF per floor at the center of mass. Each nonlinear isolation bearing or device is modeled explicitly using discrete biaxial Bouc–Wen model, and the forces in the bearings or devices are transformed to the center of mass of the base using a rigid base slab assumption. All the linear isolation bearings or devices can be modeled individually or globally by equivalent lumped elements at the center of mass of the base. The equations of motion (Figure 3) for the elastic superstructure are expressed in the following form:

$$\mathbf{M}_{n\times n}\ddot{\mathbf{U}}_{n\times 1} + \mathbf{C}_{n\times n}\dot{\mathbf{U}}_{n\times 1} + \mathbf{K}_{n\times n}\mathbf{U}_{n\times 1} = -\mathbf{M}_{n\times n}\mathbf{R}_{n\times 3}(\ddot{\mathbf{U}}_{\mathrm{g}} + \ddot{\mathbf{U}}_{\mathrm{b}})_{3\times 1} \tag{6}$$

in which n is three times the number of floors (excluding base), $\mathbf{M}$ is the superstructure mass matrix, $\mathbf{C}$ is the superstructure damping matrix in the fixed-base case, $\mathbf{K}$ is the superstructure stiffness matrix in the fixed-base case and $\mathbf{R}$ is the matrix of earthquake influence coefficients, i.e. the matrix of displacements and rotation at the center of mass of the floors resulting from a unit translation in the x and y directions and unit rotation at the center

DOI: 10.1002/stc

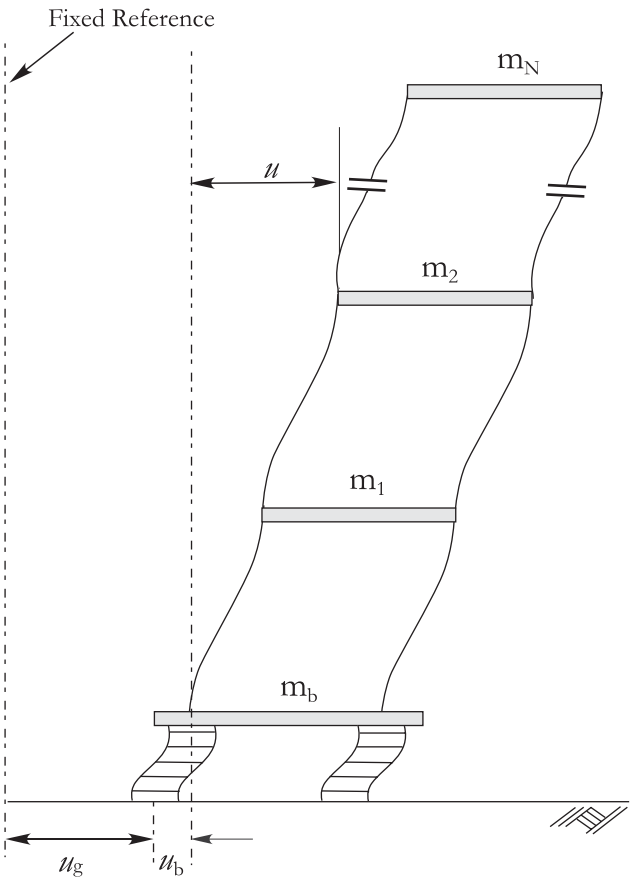

Figure 3. The displacement coordinates used to formulate the equations of motion.

of mass of the base. Furthermore, $\ddot{\mathbf{U}}$, $\dot{\mathbf{U}}$ and $\mathbf{U}$ represent the floor acceleration, velocity and displacement vectors relative to the base, $\ddot{\mathbf{U}}_b$ is the vector of base acceleration relative to the ground and $\ddot{\mathbf{U}}_g$ is the vector of ground acceleration. The equations of motion for the base are as follows:

$$\mathbf{R}_{3\times n}^{T}\mathbf{M}_{n\times n}[(\ddot{\mathbf{U}})_{n\times 1}+\mathbf{R}_{n\times 3}(\ddot{\mathbf{U}}_g+\ddot{\mathbf{U}}_b)_{3\times 1}]_{n\times 1}+\mathbf{M}_{b_{3\times 3}}(\ddot{\mathbf{U}}_g+\ddot{\mathbf{U}}_b)_{3\times 1}+\mathbf{C}_{b_{3\times 3}}\dot{\mathbf{U}}_{b_{3\times 1}}+\mathbf{K}_{b_{3\times 3}}\mathbf{U}_{b_{3\times 1}}+\mathbf{f}_{3\times 1}=0 \quad (7)$$

in which $\mathbf{M}_b$ is the diagonal mass matrix of the rigid base, $\mathbf{C}_b$ is the resultant damping matrix of viscous isolation elements, $\mathbf{K}_b$ is the resultant stiffness matrix of elastic isolation elements and $\mathbf{f}$ is the vector containing the nonlinear bearing and device forces and control forces. Equation (6) can be reformulated in the modal domain and the fixed-base frequencies, damping ratios and modes can be used for modeling the superstructure [27]. Using $\mathbf{X}=\{\mathbf{U}^T\ \mathbf{U}_b^T\ \dot{\mathbf{U}}^T\ \dot{\mathbf{U}}_b^T\}^T$, the state space equations can be formulated as

$$\dot{\mathbf{X}}(t)=\mathbf{A}\mathbf{X}(t)+\mathbf{B}\mathbf{u}(t)+\mathbf{E}\ddot{\mathbf{U}}_g(t)=\mathbf{g}(\mathbf{X},\mathbf{u},\ddot{\mathbf{U}}_g) \quad (8)$$

DOI: 10.1002/stc

$$\mathbf{A} = \begin{bmatrix} \mathbf{0} & \mathbf{I} \\ -\overline{\mathbf{M}}^{-1}\overline{\mathbf{K}} & -\overline{\mathbf{M}}^{-1}\overline{\mathbf{C}} \end{bmatrix}, \quad \mathbf{B} = \begin{bmatrix} \mathbf{0} \\ \mathbf{I} \end{bmatrix}, \quad \mathbf{E} = \begin{bmatrix} \mathbf{0} \\ -\begin{Bmatrix} \mathbf{MR} \\ \mathbf{R}^{\mathrm{T}}\mathbf{MR} + \mathbf{M}_{\mathrm{b}} \end{Bmatrix} \end{bmatrix} \tag{9}$$

$$\overline{\mathbf{M}} = \begin{bmatrix} \mathbf{M} & \mathbf{MR} \\ \mathbf{R}^{\mathrm{T}}\mathbf{M} & \mathbf{R}^{\mathrm{T}}\mathbf{MR} + \mathbf{M}_{\mathrm{b}} \end{bmatrix}, \quad \overline{\mathbf{C}} = \begin{bmatrix} \mathbf{C} & \mathbf{0} \\ \mathbf{0} & \mathbf{C}_{\mathrm{b}} \end{bmatrix} \tag{10}$$

$$\overline{\mathbf{K}} = \begin{bmatrix} \mathbf{K} & \mathbf{0} \\ \mathbf{0} & \mathbf{K}_{\mathrm{b}} \end{bmatrix}, \quad \mathbf{u} = \begin{bmatrix} \mathbf{0} \\ \mathbf{f} \end{bmatrix} \tag{11}$$

In the above equations, **A**, **B** and **E** are condensed system matrices having 54 states derived from the full three-dimensional finite element model. Equation (8) is solved using unconditionally stable Newmark's constant-average acceleration method, which can also be derived from trapezoidal rule given by

$$\mathbf{X}_{k+1} = \mathbf{X}_k + \frac{\Delta t}{2}(\mathbf{g}_k + \mathbf{g}_{k+1}) \tag{12}$$

where $\mathbf{g}_{k+1} = \mathbf{g}(\mathbf{X}_{k+1}, \mathbf{u}_{k+1}, \ddot{\mathbf{U}}_{g_{(k+1)}})$. This method is implicit, needing iteration. The nonlinear forces in the isolation bearings, devices and control forces are updated by solving Equations (1)–(5) using the unconditionally stable semi-implicit Runge–Kutta method suitable for solutions of stiff differential equations. Then Equation (8) is re-solved using an iterative predictor–corrector solution procedure [27] until equilibrium of nonlinear forces is reached within specified tolerance and convergence is achieved. The nonlinear analysis program is implemented as an S-function, written in C programing language, within the SIMULINK [28] environment.

4. MATLAB IMPLEMENTATION

The analysis program comprises of input data files, a file to read and assemble the required matrices for input into the nonlinear dynamic analysis block, which is a SIMULINK-based S-function program. Additional inputs to the nonlinear analysis block are the seismic excitation and the control forces provided by the control devices. All the sensor and control devices can be modeled in this program as SIMULINK blocks and the outputs of these models fed into the analysis S-function block. The benchmark study participants are to define the type, the appropriate model and the location of the sensor(s), the control devices and the control algorithms. The analysis program will remain invariant to the various control strategies developed and implemented. The various control strategies can be compared with one another by having the model and evaluation criteria common to all controllers. The control devices, sensor devices and the control algorithms can be interfaced to the structural evaluation model though measurement and device connection outputs. The evaluation outputs are used for the calculation of performance indices. Detailed discussion of the numerical implementation can be found in the Phase I benchmark definition paper by the authors [3] and the SIMULINK model used for Phase II simulations (for the friction isolation system) is shown in Figure 4.

DOI: 10.1002/stc

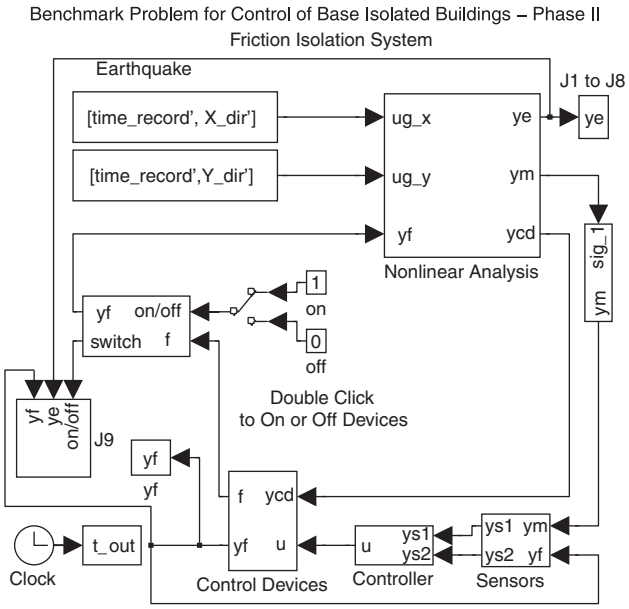

Figure 4. SIMULINK model used for Phase II simulations.

5. EVALUATION CRITERIA

A set of near-fault earthquake excitations are considered for evaluation purposes as shown in Figure 5. The earthquakes used in this study are Newhall (1994 Northridge Earthquake, Newhall county, fault-normal 360° and fault-parallel 90°), Sylmar (1994 Northridge Earthquake, Sylmar station, fault-normal 360° and fault-parallel 90°), El Centro (1994 Northridge Earthquake, El Centro record, fault-normal and fault-parallel), Rinaldi (1994 Northridge Earthquake, Rinaldi station, fault-normal 228° and fault-parallel 318°), Kobe (1995, JMA station, East–West and North–South components), Jiji (1999, station TCU 068, East–West and North–South components) and Erzinkan (1992, 1719, Turkey, East–West and North–South components). A set of nine performance indices, $J1$–$J9$, given in Table I are used to assess the performance of the control designs [3]. The indices $J1$–$J5$ measure the peak values of base shear, structural shear, base displacement, inter-story drift and floor accelerations, respectively. These values are normalized by their respective uncontrolled values; 'uncontrolled' refers to the case when there is no force feedback to the structure and the control device (active, passive or semiactive) is disconnected from the structural system. The performance index $J6$ measures the maximum control force developed in the device normalized with respect to the peak base shear. The indices $J7$ and $J8$ measure the root mean square values of displacement and base acceleration normalized by their uncontrolled values. The index $J9$ measures the energy dissipated by the semiactive device as a percentage of the input excitation energy.

The main objective of the controller designs is to reduce the values of the performance indices, especially $J1$–$J8$; lower values indicate better controller performance. However, lower values of the index $J6$ may sometimes be indicative of lower base shears, in which case the results must be interpreted accordingly. In the following discussion, a semiactive controller

DOI: 10.1002/stc

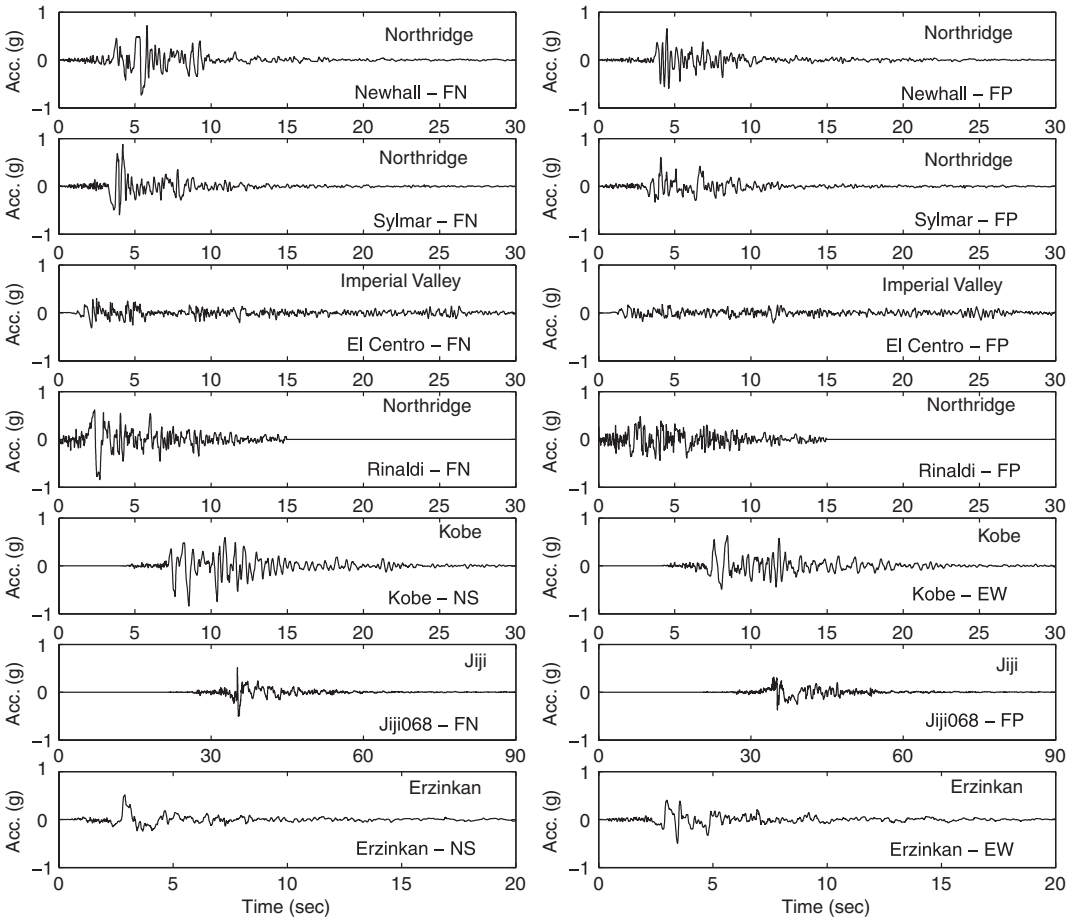

Figure 5. Earthquakes used for the Phase II simulation study.

Table I. Performance indices.

Peak base shear*	Peak structure shear*	Peak base displacement*
$J1=\dfrac{\max_t \lVert V_0(t)\rVert}{\max_t \lVert \hat{V}_0(t)\rVert}$	$J2=\dfrac{\max_t \lVert V_1(t)\rVert}{\max_t \lVert \hat{V}_1(t)\rVert}$	$J3=\dfrac{\max_t \lVert x_b(t)\rVert}{\max_t \lVert \hat{x}_b(t)\rVert}$
Peak inter-story drift*	Peak floor acceleration*	Peak control force
$J4=\dfrac{\max_{t,f} \lVert d_f(t)\rVert}{\max_{t,f} \lVert \hat{d}_f(t)\rVert}$	$J5=\dfrac{\max_{t,f} \lVert a_f(t)\rVert}{\max_{t,f} \lVert \hat{a}_f(t)\rVert}$	$J6=\dfrac{\max_t \lVert f_d(t)\rVert}{\max_t \lVert \hat{V}_0(t)\rVert}$
RMS base displacement*	RMS floor acceleration*	Energy dissipated by devices
$J7=\dfrac{\max_i \lVert \sigma_d(t)\rVert}{\max_i \lVert \sigma_{\hat{d}}(t)\rVert}$	$J8=\dfrac{\max_f \lVert \sigma_a(t)\rVert}{\max_f \lVert \sigma_{\hat{a}}(t)\rVert}$	$J9=\dfrac{[\int_0^T f_d(t)\dot{x}_b(t)\,\mathrm{d}t]}{\int_0^T \langle V_0(t)\dot{U}_g(t)\rangle\,\mathrm{d}t}$

*The denominator consists of the corresponding response quantity in the uncontrolled case. f, *floor*, number, 1,…,8; t, time, $0 \le t \le T$; $\langle\cdot\rangle$ inner product; $\lVert\cdot\rVert$ vector magnitude; V_0, V_1, base and structural shears; x_b, base displacement; d_f, inter-story; drift; a_f, floor acceration; σ_d and σ_a and RMS base displacement and floor acceleration; corresponding response quantity in the uncontrolled case.

DOI: 10.1002/stc

using variable dampers is derived using a Lyapunov formulation to control the responses of the friction isolation case and results are presented in terms of these performance indices.

6. SEMIACTIVE LYAPUNOV CONTROLLER FOR FRICTION ISOLATION SYSTEM

In order to illustrate the implementation of controllers for the friction-isolated benchmark structure, a sample semiactive Lyapunov controller is presented. MR dampers are employed in order to control the response of the structure. The Lyapunov semiactive control algorithm [16] is developed based on energy principles for a general ground-excited spring–mass–dashpot system with time-varying damping. The base-isolated structure behaves predominantly in its first mode and the response characteristics are similar to the response of a single DOF system. For such a vibration in its predominant mode, with system parameters consisting of mass m, stiffness k and a time-varying damping $c(t)$, the equations of motion can be written in state space as follows:

$$\dot{X} = AX - Bc(t)\dot{u}_r + Bku_g - Bf_c \tag{13}$$

where

$$A = \begin{bmatrix} 0 & 1 \\ \frac{-k}{m} & 0 \end{bmatrix} \tag{14}$$

$$B = \begin{Bmatrix} 0 \\ \frac{1}{m} \end{Bmatrix} \tag{15}$$

$$X = \begin{Bmatrix} u_a \\ \dot{u}_a \end{Bmatrix} \tag{16}$$

In the above equations, u_a and $\dot{u}_a$ denote the absolute displacement and the absolute velocity, respectively, u_r is the relative displacement, f_c is the nonlinear isolation force and u_g denotes the ground displacement. A scalar Lyapunov function (V) is defined as

$$V = \tfrac{1}{2}\sigma^T(X)\sigma(X) \tag{17}$$

where

$$\sigma(X) = P^T X = [\sqrt{k} \;\; \sqrt{m}] \begin{Bmatrix} u_a \\ \dot{u}_a \end{Bmatrix} \tag{18}$$

where P is a constant vector.

Hence, the Lyapunov function V can now be written as

$$V = \tfrac{1}{2}ku_a^2 + \sqrt{k}\sqrt{m}u_a\dot{u}_a + \tfrac{1}{2}m\dot{u}_a^2 \tag{19}$$

where the first term represents the total strain energy in the spring, second term represents the dissipated energy and the third term represents the total kinetic energy.

Differentiating Equation (19), and substituting Equation (13), we get

$$\dot{V} = \sigma(X)P^T B\dot{u}_r\left(-c(t) + \frac{1}{\dot{u}_r}(\sqrt{k}\sqrt{m}\dot{u}_a - ku_r - f_s)\right) \tag{20}$$

DOI: 10.1002/stc

For $\dot{V}$ to be negative, the following condition should be satisfied:

$$c(t) = \begin{cases} c_2 \text{ or } c_{\max} & (\sqrt{k}u_a + \sqrt{m}\dot{u}_a)\dot{u}_r > 0 \\ c_1 \text{ or } c_{\min} & (\sqrt{k}u_a + \sqrt{m}\dot{u}_a)\dot{u}_r < 0 \end{cases} \tag{21}$$

Equation (21) can also be written as

$$c(t) = \begin{cases} c_2 \text{ or } c_{\max} & (\omega_n u_a + \dot{u}_a)\dot{u}_r > 0 \\ c_1 \text{ or } c_{\min} & (\omega_n u_a + \dot{u}_a)\dot{u}_r < 0 \end{cases} \tag{22}$$

where $\omega_n = \sqrt{k/m}$, $u_a(t)$ is the absolute displacement and $\dot{u}_r(t)$ is the relative velocity of the structure. A total of 18 acceleration sensors are used for measurements: eight orthogonal pairs of accelerometers at the eight device locations and two accelerometers to measure the ground excitation in two directions. Note that the control switching laws in Equation (22) require absolute velocity and absolute displacement in addition to the relative velocity. In the benchmark programs, the relative velocity at the base is an admissible measurement. However, the absolute velocities and displacements are obtained by using a filter that mimics an integrator [8]. Details of the MR damper model and parameters have been presented elsewhere [8, 29]. For the ensuing simulations, the value of $\omega_n = 2.1$ rad/s is used corresponding to the natural period of the linear isolated structure. Two centralized controllers operating independently in each principal direction of the structure located at the center of mass of the base are utilized to generate the controller command voltages. The controller command voltage so developed at the center of mass in response to the structure responses is then used to switch the devices at all the locations uniformly.

6.1. Results of the simulations

The results of the sample Lyapunov controller are presented in Tables II and III in terms of the performance indices defined earlier. Since the sample controller is semiactive, for comparison purposes, results when the semiactive device is set in its passive mode (maximum voltage to the MR damper at all times) are presented in Tables IV and V, respectively. The performance indices for the uncontrolled case (no semiactive devices at the isolation level) are presented in Tables VI and VII.

Though the results presented in this paper are not intended to be competitive, it is useful to briefly discuss the results and some of the issues regarding the control of nonlinear base-isolated buildings. From the performance indices presented in Tables II and III, it is clear that the peak

Table II. Results for Lyapunov control-friction isolation (FP—x and FN—y).

	$J1$	$J2$	$J3$	$J4$	$J5$	$J6$	$J7$	$J8$	$J9$
Newhall	1.02	0.93	0.70	1.20	1.16	0.29	0.56	1.36	0.44
Sylmar	0.99	1.02	0.75	1.13	1.56	0.24	0.58	1.33	0.47
El Centro	1.28	1.21	0.48	1.24	1.26	0.43	1.05	1.37	0.43
Rinaldi	0.95	0.92	0.80	1.02	1.73	0.27	0.75	1.53	0.44
Kobe	1.12	1.26	0.61	1.37	1.56	0.32	0.65	1.38	0.43
Jiji	0.85	0.86	0.72	0.95	1.30	0.17	0.71	1.61	0.33
Erzinkan	0.98	0.99	0.70	1.03	1.40	0.26	0.61	1.12	0.48

DOI: 10.1002/stc

Table III. Results for Lyapunov control-friction isolation (FN—x and FP—y).

	$J1$	$J2$	$J3$	$J4$	$J5$	$J6$	$J7$	$J8$	$J9$
Newhall	1.02	0.89	0.72	1.11	1.28	0.29	0.56	1.31	0.44
Sylmar	1.00	1.04	0.79	0.92	1.62	0.23	0.59	1.19	0.47
El Centro	1.44	1.24	0.77	1.20	1.29	0.40	0.89	1.29	0.42
Rinaldi	0.92	0.88	0.76	0.93	1.34	0.30	0.79	1.85	0.44
Kobe	1.18	1.14	0.55	1.39	1.53	0.31	0.62	1.36	0.42
Jiji	0.86	0.87	0.71	0.90	0.95	0.17	0.68	1.13	0.34
Erzinkan	1.01	0.99	0.59	1.04	1.56	0.25	0.51	1.06	0.48

Table IV. Results for passive MRD-friction isolation (FP—x and FN—y).

	$J1$	$J2$	$J3$	$J4$	$J5$	$J6$	$J7$	$J8$	$J9$
Newhall	1.04	1.06	0.67	1.37	1.22	0.32	0.60	1.46	0.52
Sylmar	0.99	1.02	0.74	1.25	1.81	0.25	0.57	1.41	0.51
El Centro	1.43	1.38	0.45	1.68	1.34	0.39	1.19	1.46	0.56
Rinaldi	1.05	1.04	0.77	1.20	2.13	0.27	0.82	1.71	0.52
Kobe	1.12	1.43	0.61	1.69	1.78	0.35	0.70	1.55	0.50
Jiji	0.81	0.82	0.67	0.98	1.38	0.18	0.58	1.44	0.46
Erzinkan	1.04	1.07	0.74	1.15	1.66	0.25	0.68	1.28	0.52

Table V. Results for passive MRD-friction isolation (FP—y and FN—x).

	$J1$	$J2$	$J3$	$J4$	$J5$	$J6$	$J7$	$J8$	$J9$
Newhall	1.02	1.05	0.70	1.36	1.64	0.30	0.61	1.44	0.51
Sylmar	1.02	1.07	0.80	1.09	1.97	0.23	0.59	1.28	0.51
El Centro	1.46	1.51	0.52	1.51	1.45	0.41	1.11	1.40	0.56
Rinaldi	1.04	1.01	0.75	1.07	1.44	0.27	0.88	1.63	0.52
Kobe	1.19	1.29	0.57	1.70	1.74	0.33	0.75	1.53	0.50
Jiji	0.79	0.81	0.63	0.85	1.07	0.18	0.54	1.28	0.46
Erzinkan	1.10	1.02	0.64	1.05	1.46	0.24	0.58	1.16	0.53

Table VI. Uncontrolled response quantities for friction isolation system (FP—x and FN—y).

	Newhall	Sylmar	El Centro	Rinaldi	Kobe	Jiji	Erzinkan
Peak base shear (norm. by W^*)	0.170	0.245	0.083	0.228	0.140	0.424	0.220
Peak str. shear (norm. by W^*)	0.151	0.213	0.086	0.199	0.110	0.352	0.180
Peak isolator deformation (m)	0.300	0.489	0.108	0.433	0.252	1.095	0.512
Peak I. S drift (norm. by h^*)	0.002	0.003	0.002	0.003	0.002	0.004	0.003
Peak absolute acc. (g^*)	0.572	0.355	0.402	0.338	0.360	0.478	0.270
RMS disp. (m)	0.071	0.124	0.023	0.084	0.050	0.166	0.151
RMS acc. (g^*)	0.080	0.076	0.079	0.071	0.083	0.071	0.074

*W, weight of the structure (202 000 kN); h, average story height (4.04 m); g, acceleration due to gravity (9.81 m/s^2).

DOI: 10.1002/stc

Table VII. Uncontrolled response quantities for friction isolation system (FP—y and FN—x).

	Newhall	Sylmar	El Centro	Rinaldi	Kobe	Jiji	Erzinkan
Peak base shear (norm. by W^*)	0.177	0.251	0.080	0.232	0.140	0.428	0.225
Peak str. shear (norm. by W^*)	0.162	0.205	0.087	0.201	0.119	0.363	0.195
Peak isolator deformation (m)	0.292	0.495	0.085	0.428	0.281	1.188	0.563
Peak I. S drift (norm. by h^*)	0.003	0.003	0.002	0.003	0.002	0.005	0.003
Peak absolute acc. (g^*)	0.464	0.434	0.375	0.377	0.368	0.493	0.319
RMS disp. (m)	0.068	0.133	0.020	0.084	0.051	0.182	0.168
RMS acc. (g^*)	0.081	0.079	0.079	0.068	0.082	0.076	0.082

*W, weight of the structure (202 000 kN); h, average story height (4.04 m); g, acceleration due to gravity (9.81 m/s^2).

base displacements ($J3$) are reduced considerably by the addition of control beyond uncontrolled values. However, this reduction in the peak base displacements occurs at the cost of increased superstructure accelerations reflected in the indices $J1$, $J2$ and $J5$, where many response quantities are higher than one. However, the benefits of control are clearly evident if the results in Tables II and III are compared with results of passive case in Tables IV and V. For example, some performance indices for the passive case are greater than 2 (Table IV, Rinaldi—$J5$). However, the results for the controlled case are lower than the passive case, while achieving similar magnitude reductions in the base displacements ($J3$). These results clearly demonstrate the need to design effective active and semiactive control strategies, as passive control alone may not provide the necessary means to achieve the performance objectives in nonlinear base-isolated buildings. Clearly, performance indices greater than one for the response quantities are not desirable; it is emphasized that for the control schemes to be competitive, participants should strive toward controller designs that yield relatively low values of the performance indices.

Time-history results for Sylmar Earthquake are presented in Figure 6 for the controlled, passive and uncontrolled cases. The response time histories of the roof acceleration, base displacement and the control force are presented along with the force–displacement loops for the total isolation level force (transformed to the center of mass of the base). The effects of semiactive control are evident in Figure 6 where the base displacements for the passive and controlled cases are significantly lower than the uncontrolled values, while the accelerations are at or above their uncontrolled counterparts. The force–displacement characteristics for a typical friction isolator and an MR damper located near the center of mass of the base are shown in Figure 7 demonstrating the control action during periods of peak responses.

7. SAMPLE CONTROLLER FOR THE BILINEAR LRB ISOLATION SYSTEM

As noted earlier, the focus of Phase II effort is on friction and LRB isolation systems. The sample controller for the friction isolation system has been presented in the earlier sections. For the LRB isolation system, a Linear Quadratic Gaussian (LQG) controller is designed for an equivalent linear system such that the equivalent linear system and the nonlinear benchmark system have similar response characteristics when controlled. An iterative procedure is developed to satisfy a criterion that is based on the similarity of the forces associated with the nonlinear elements in the linear and nonlinear systems. Results for the iterative procedure are

DOI: 10.1002/stc

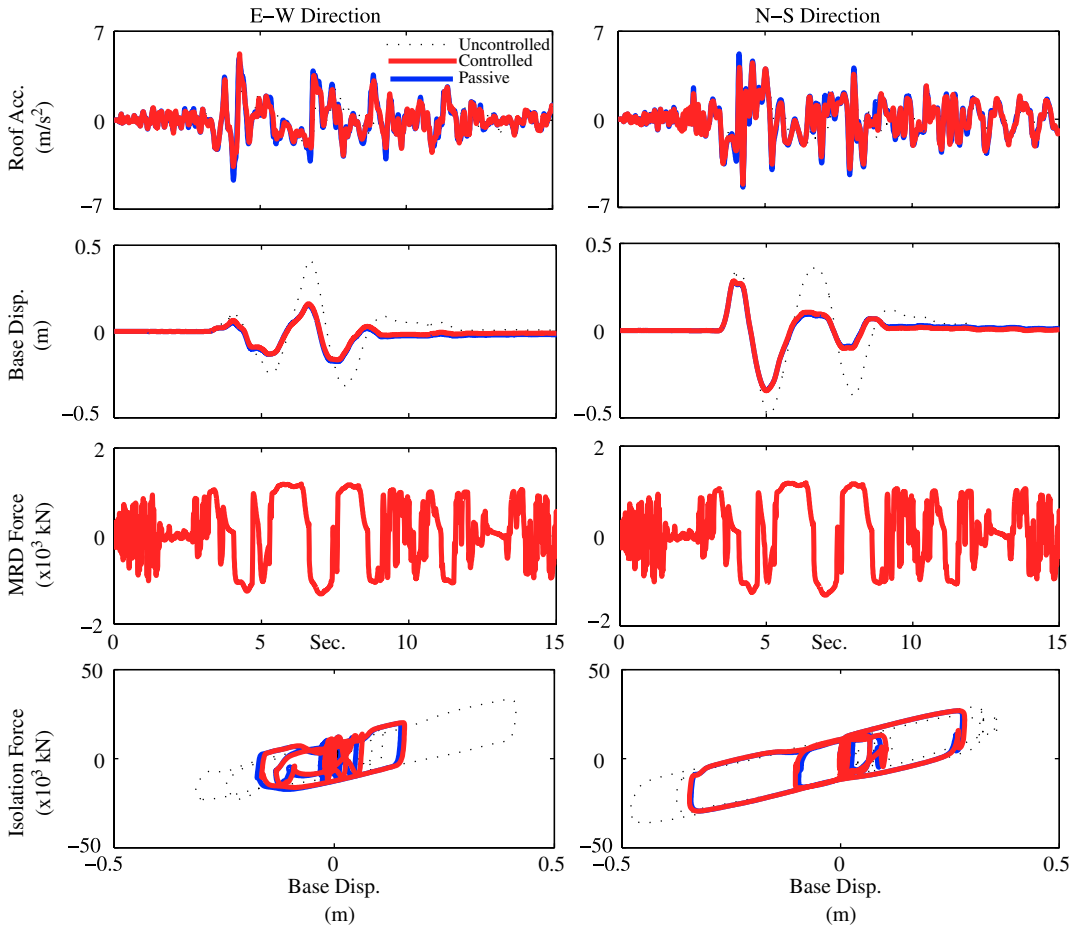

Figure 6. Results of Lyapunov controller for Sylmar Earthquake—response time histories of roof accelerations, MRD force commanded by the controller at the CM of the base and total isolation force at the center of mass of base.

given for several earthquakes and, based on these results, the final LQG controller and the corresponding equivalent linear structure parameters are presented [9]. The participants for the Phase II study are referred to a separate study for the details [9].

8. CONCLUSIONS

In this paper, a sample controller for the Phase II smart nonlinear base isolation benchmark problem for the friction isolation system is presented. While the primary focus of the first phase was on linear isolation system and linear controllers, the main objective of the Phase II of the benchmark is on nonlinear isolation systems. Specifically, friction pendulum and hysteretic LRBs are considered in the Phase II study. As with the

DOI: 10.1002/stc

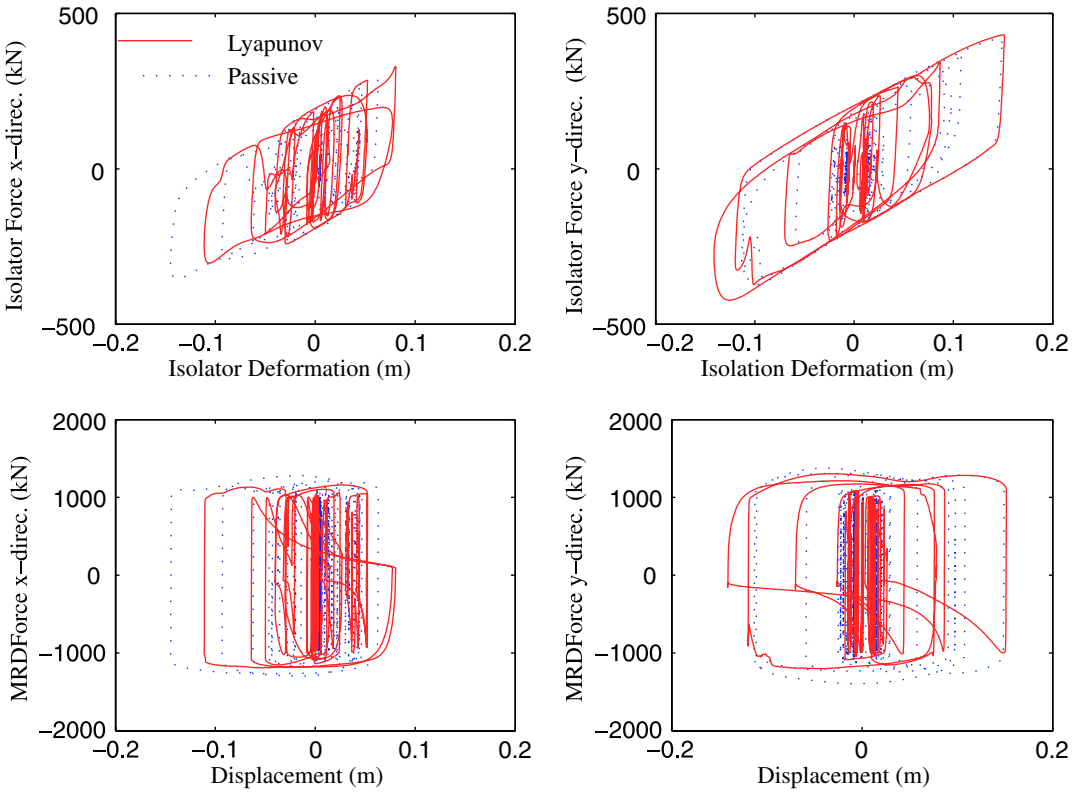

Figure 7. Force–displacement loops in x (East–West) and y (North–South) directions for the isolator and MR damper near the center of the base for Kobe Earthquake FP—x and FN—y.

Phase I, the superstructure remains linear. The programs developed and distributed to the participants of this study have the flexibility to incorporate a host of active, passive and semiactive devices at the isolation level. A Lyapunov semiactive controller is developed for the friction isolation system with time-varying damping. The results of the simulation study are presented in the form of a set of performance indices. The need for effective controllers and some of the performance issues with the semiactive control of nonlinear base-isolated buildings was demonstrated. The control design presented in this study is intended to be an aid for the benchmark problem participants to design nonlinear controllers; it is expected that results can be improved further by designing more effective controllers.

ACKNOWLEDGEMENTS

The authors would like to acknowledge the funding provided by National Science Foundation. The first author gratefully acknowledges the funding provided by the University of Waterloo and the Natural Sciences and Engineering Research Council (NSERC) of Canada.

DOI: 10.1002/stc

REFERENCES

1. Agrawal AK, Tan P, Nagarajaiah S, Zhang J. Benchmark structural control problem for a seismically excited highway bridge, part I: problem definition, http://www-ce.engr.ccny.cuny.edu/People/Agrawal, 2005.
2. Dyke SJ, Caicedo JM, Turan G, Bergman LA, Hague S. Phase I: benchmark control problem for seismic response of cable stayed bridges. *Journal of Structural Engineering* (ASCE) 2003; **129**(7):857–872.
3. Narasimhan S, Nagarajaiah S, Gavin H, Johnson EA. Smart base isolated benchmark building part I: problem definition. *Journal of Structural Control and Health Monitoring* 2006; **13**(2–3):573–588.
4. Ohtori Y, Christenson RE, Spencer BF, Dyke SJ. Benchmark problems in seismically excited nonlinear buildings. *Journal of Engineering Mechanics* (ASCE) 2004; **130**(4):366–385.
5. Spencer BF, Dyke SJ, Deoskar HS. Benchmark problems in structural control: part 2—active tendon system. *Earthquake Engineering and Structural Dynamics* 1998; **27**(11):1127–1147.
6. Tan P, Agrawal AK. Benchmark structural control problem for a seismically excited highway bridge, part II: sample control designs, http://www-ce.engr.ccny.cuny.edu/People/Agrawal, 2005.
7. Yang JN, Agrawal A, Samali B, Wu JC. A benchmark problem for response control of wind excited tall buildings. *Journal of Engineering Mechanics* (ASCE) 2004; **130**(4):437–446.
8. Nagarajaiah S, Narasimhan S. Smart base isolated benchmark building part II: phase I sample controllers for linear isolation system. *Journal of Structural Control and Health Monitoring* 2006; **13**(2–3):589–604.
9. Erkus B, Johnson E. Smart base isolated benchmark building part III: a sample controller for bilinear isolation. *Journal of Structural Control and Health Monitoring* 2006; **13**(2–3):605–625.
10. Narasimhan S, Nagarajaiah S. Smart base isolated buildings with variable friction systems: H_∞ controller and novel SAIVF device. *Earthquake Engineering and Structural Dynamics* 2006; **35**(8):920–942.
11. Narasimhan S, Nagarajaiah S. STFT algorithm for semiactive control of base isolated buildings with variable stiffness isolation systems subjected to near fault earthquakes. *Engineering Structures* 2005; **27**:514–523.
12. Spencer BF, Nagarajaiah S. State of the art of structural control. *Journal of Structural Engineering* 2003; **129**(7):845–856.
13. Nagarajaiah S, Saharabudhe S. Seismic response control of smart sliding isolated buildings using variable stiffness systems: experimental and numerical study. *Earthquake Engineering and Structural Dynamics* 2006; **35**(2):177–197.
14. Nagarajaiah S, Narasimhan S. Seismic control of smart base isolated buildings with new semiactive variable damper. *Earthquake Engineering and Structural Dynamics* 2007; **36**(6):729–749.
15. Nagarajaiah S, Mao YQ, Sahasrabudhe S. Nonlinear, seismic response spectra of smart sliding isolated structures with independently variable MR dampers and variable stiffness SAIVS system. *Journal of Structural Engineering and Mechanics* 2006; **24**(3):375–393.
16. Sahasrabudhe S, Nagarajaiah S. Semi-active control of sliding isolated bridges using MR dampers: an experimental and numerical study. *Earthquake Engineering and Structural Dynamics* 2005; **34**(8):965–983.
17. Yang JN, Li Z, Wu JC, Hsu IR. Control of sliding-isolated buildings using dynamic linearization. *Journal of Engineering Structures* 1994; **16**(6):437–444.
18. Yang JN, Wu J, Reinhorn A, Riley M. Control of sliding-isolated buildings using sliding-mode control. *Journal of Structural Engineering* (ASCE) 1996; **122**:179–186.
19. Yang JN, Agrawal AK. Semi-active hybrid control systems for nonlinear buildings against near-field earthquakes. *Engineering Structures* 2002; **24**(3):271–280.
20. Yang JN, Wu J, Kawashima K, Unjoh S. Hybrid control of seismic-excited bridge structures. *Earthquake Engineering and Structural Dynamics* 1995; **24**(11):1437–1451.
21. Wongprasert N, Symans MD. Experimental evaluation of adaptive elastomeric base-isolated structures using variable-orifice fluid dampers. *Journal of Structural Engineering* (ASCE) 2005; **131**(6):867–877.
22. Yang JN, Lin S, Jabbari F. H_2 based control strategies for civil engineering structures. *Journal of Structural Control and Health Monitoring* 2003; **11**(3):223–237.
23. Yang JN, Lin S, Jabbari F. H_∞ based control strategies for civil engineering structures. *Journal of Structural Control* 2004; **10**:205–230.
24. Carlson JD, Chrzan MJ. Magnetorheological fluid dampers. *U.S. Patent No. 5,277,281*, 1994.
25. Wen YK. Method of random vibration of hysteretic systems. *Journal of Engineering Mechanics* (ASCE) 1976; **102**(2):249–263.
26. Park YJ, Wen YK, Ang AHS. Random vibration of hysteretic systems under bi-directional ground motions. *Earthquake Engineering and Structural Dynamics* 1986; **14**(4):543–557.
27. Nagarajaiah S, Reinhorn AM, Constantinou MC. Nonlinear dynamic analysis of 3-d-base-isolated structures. *Journal of Structural Engineering* (ASCE) 1991; **117**(7):2035–2054.
28. MATLAB. The Math Works, Inc., Natick, MA, 2000.
29. Spencer BF, Dyke SJ, Sain MK, Carlson JD. Phenomenological model of a magnetorheological damper. *Journal of Engineering Mechanics* 1997; **123**(3):230–238.

DOI: 10.1002/stc